Consequences of Nitrogen-Doping and Oxygen Enrichment on Titanium Local Order and Photocatalytic Performance of TiO_2 Anatase

Igor Krivtsov[1,2], Marina Ilkaeva[1,2], Eduardo Salas-Colera[3,4], Zakariae Amghouz[5], José R. García[1], Eva Díaz[6], Salvador Ordóñez[6], Silvia Villar-Rodil[7]*

[1] Department of Organic and Inorganic Chemistry, University of Oviedo-CINN, 33006 Oviedo, Spain.

[2]Nanotechnology Education and Research Center, South Ural State University, 454080, Chelyabinsk, Russia.

[3] Instituto de Ciencia de Materiales de Madrid, CSIC, Sor Juana Inés de la Cruz 3, 28049, Cantoblanco Madrid, Spain.

[4] Spanish CRG BM25 SpLine Beamline at the ESRF, 71 Avenue de Martyrs, F-38043 Grenoble, France.

[5] Servicios Científico Técnicos, University of Oviedo-CINN, 33006 Oviedo, Spain

[6] Department of Chemical and Environmental Engineering, University of Oviedo, 33006 Oviedo, Spain

[7]Instituto Nacional del Carbón, INCAR-CSIC, Apartado 73, 33080, Oviedo, Spain

ABSTRACT

Extended X-ray Absorption Fine Structure (EXAFS) investigation of the oxygen-rich titania formed *via* the thermal treatment of N-doped TiO_2 has revealed that the removal of N-dopants is responsible for the creation of defect sites in the titanium environment, thus triggering at high temperatures (500-800 ^oC) the capture of atmospheric oxygen followed by its diffusion towards the vacant sites and formation of interstitial oxygen species. The effect of the dopants on Ti coordination number and Ti-O_{int} and Ti-N_{int} bond distances has been estimated. The photocatalytic *p*-cresol degradation tests have demonstrated that the interband states formed by the N-dopants contribute to a greater extent to the visible-light activity than the oxygen interstitials do. However, under the UV irradiation the oxygen-rich titania shows higher efficiency in the pollutant degradation, while the N-dopants in N-TiO_2 play the role of recombination sites. On the other hand, the presence of the surface nitrogen species in TiO_2 is highly beneficial for the application in partial photooxidation reactions, where N-TiO_2 demonstrates a superior selectivity of 5-hydroxymethyl furfural (HMF) oxidation to 2,5-furandicarboxaldehyde (FDC). Thus, this work underlines the importance of a rational design of non-metal doped titania for photocatalytic degradation and partial oxidation applications, and it establishes the role of bulk defects and surface dopants on the TiO_2 photooxidation performance.

1. INTRODUCTION

Titanium dioxide is a well-known photocatalyst efficient under UV irradiation[1-4], although nowadays the extension of its photocatalytic properties to a broader part of the solar spectrum is of key interest[5-8]. This can be achieved by nitrogen-doping[9], oxygen-vacancies creation[10], H_2O_2-modification[11] or oxygen interstitials incorporation[12]. The formation of the interstitial oxygen species is observed for different metal oxide materials[13-16]. The presence of interstitial oxygen in TiO_2 was proposed on the basis of theoretical calculations[17-19] and confirmed experimentally for the reduced TiO_2 having Ti^{3+} sites[20], rutile single crystal with oxygen vacancies[21], and it was even observed by the electron microscopy methods for Nb-doped TiO_2[22]. The common feature of the reported TiO_2 materials containing oxygen interstitials is their defective structure formed as the result of doping, reductive or high-energy treatment. The presence of structural defects drives O_2 capture and its consecutive incorporation into TiO_2 crystals aiming to compensate the net-charge imbalance. Etacheri *et al*[12] reported an intriguing procedure for the preparation of the visible-light active oxygen-rich TiO_2 anatase, where the only dopant was the interstitial oxygen incorporated into the oxide structure under calcination. Latter, Tan *et al*[23-25] described a series of the preparation procedures devoted to obtain the oxygen-rich titania guided mostly by the H_2O_2:Ti ratio suggested in[12], while using a different TiO_2 source. However, the properties i.e. phase composition and band-gap energy of the materials synthesized by Tan *et al* did not coincide with those reported in[12], thus forcing us to rethink the mechanism of oxygen-rich titania formation. Earlier in[26], we established that a similar preparation procedure reported in[12] led to N-doping of titania at treatment temperatures up to 500 ^oC. The N-species can occupy substitutional or interstitial positions in TiO_2 network, as demonstrated by spectroscopic studies[27,28]. Belver *et al*[29, 30] were the first in providing a deeper insight in the local arrangement

of Ti in the N-doped titania, using more sophisticated analytical methods as *in-situ* DRIFT studies and XAS investigation. They discovered that the N-doping was responsible for the oxygen-vacancies formation in titanium dioxide. In a more recent investigation supported by DFT calculations and EXAFS, Ceotto *et al* postulated that nitrogen preferentially occupies the axial position in the TiO_6 polyhedra replacing the lattice oxygen at low doping levels and forming oxygen-vacancies at high dopant concentrations[31]. Several years later, Sahoo *et al* found out by means of EXAFS that the nitrogen interstitial doping is responsible for the reduction of Ti-O coordination number and the increase of the axial and equatorial Ti-O bond lengths[32].

In our view, the N-doping related defects in TiO_2 might be a driving force of the consecutive O-interstitials incorporation and oxygen-rich titania formation. Here, we will explore this hypothesis focusing on evaluation of the data obtained from EXAFS and other analytical techniques about the local Ti arrangement in the titania anatase. We will also demonstrate that the type of dopants is not only responsible for the visible-light absorption, but also it determines the performance of TiO_2 in destructive and selective photocatalytic reactions. A bare TiO_2 having a hydroxylated surface is an efficient photocatalyst for the destruction of water pollutants, such as phenols[33], while achieving selectivity in partial oxidation reactions in water medium usually demands the materials to be modified by dopants or its crystallinity to be reduced[34]. Thus, we propose the rational design of doped TiO_2 targeting some specific photocatalytic applications. *p-cresol*, a phenolic compound representing a common water pollutant, and *5-hydroxymethyl-2-furfural (HMF)*, the biomass platform molecule used to produce valuable in polymer industry *2,5-furnadicarboxylic acid* and *2,5-furandicarboxyaldehyde (FDC)*[35-37]. These are not only model reactions chosen to assess the photodegradation and selective photooxidation

properties of N-doped and oxygen-rich TiO_2, but also they are processes of current interest in the field of wastewater treatment and biomass upgrading.

2. EXPERIMENTAL

Materials and Methods. Titanium oxysulfate hydrate containing 17% of H_2SO_4 was purchased from Aldrich. Ammonia 20% water solution, 30 wt% hydrogen peroxide (H_2O_2) water solution were of analytical grade and used as received without additional purification. The concentration of titanium oxysulfate was determined gravimetrically prior to its use in the synthesis. A commercial titanium dioxide (anatase phase) was purchased from Aldrich.

The titanium dioxide photocatalysts were prepared by the method described elsewhere[26], which was also similar to that described by Etacheri *et al*[12]. Despite titanium oxysulfate hydrate instead of titanium tetrachloride was used, a stable water-soluble peroxotitanium complex was eventually formed in both cases. Briefly, titanium oxysulfate hydrate containing 5 mmol of TiO_2 was dissolved in deionized water and then precipitated with 4 mL of 20 % of ammonia water solution. The resulting precipitate of titanium hydroxide was centrifuged at 3000 rpm and thoroughly washed with deionized water until the sulfates were no longer detected. On the next step of the synthesis the precipitate was dissolved by adding 3 mL of H_2O_2 (30 %) and the titanium peroxo complex was formed. Ammonia (3 M) was used to adjust pH value of the peroxo complex to 9.5, while it was ice-cold. Then, the peroxo complex solution was heated at 50 °C while stirring until the complex was gelled. The gel was dried at 70 °C overnight, powdered in an agate mortar and calcined in a muffle furnace in air at 400°C, 500 °C, 600 °C, and 800 °C. The heating rate was 3 ºC·min^{-1} and the samples were left for 2 h at the fixed

temperatures. The prepared photocatalysts were designated as T_x, where x – indicates a calcination temperature.

Characterization. Powder X-ray diffraction analysis (PXRD) was carried out using a Phillips X'pert diffractometer operating at Cu Kα radiation (λ=0.15418 nm). The mean crystal size of the TiO_2 samples was estimated by Scherrer equation from the (101) reflection of anatase phase. The amount of amorphous phase in the photocatalysts was determined by the internal standard method. The PXRD data, collected from the samples mixed with 20 wt% of CaF_2, were refined using MAUD software and the quantity of the amorphous TiO_2 was calculated using the following expression:

Comentario [Office1]: Question 1

$$W_{am} = \left(1 - \frac{W_{std}}{W_{xrd}}\right) * 100\%,$$

where W_{am} is a weight percentage of the amorphous phase, W_{std} is the fraction of CaF_2 added to the sample, and W_{xrd} is the fraction of CaF_2 in the mixture with the titania samples determined by PXRD quantitative phase analysis.

Micromeritics ASAP 2020 was used to obtain N_2 adsorption-desorption isotherms at 77 K. Before the experiment, the samples were outgassed under vacuum at 250 ºC. Specific surface area (SSA) and pore volume were calculated using BET and BJH methods. A Shimadzu UV-2700 spectrophotometer with integrated sphere attachment was used to obtain diffuse reflectance (DR) spectra of the samples using barium sulfate as a reference. Band gap (BG) energy was estimated by Kubelka-Munk method. Electron energy loss spectroscopy (EELS) studies were performed on a JEOL JEM-2100F transmission electron microscope The samples for TEM were dispersed in ethanol, sonicated and sprayed on a Holey carbon film coated copper grid and then allowed to airdry. Finally, Gatan SOLARUS 950 was used before observation. The surface composition and binding energies of Ti, O and N in the prepared photocatalysts were measured

by X-ray Photoelectron Spectroscopy (XPS), using a SPECS system equipped with a Hemispherical Phoibos analyzer operating in a constant pass energy, using Mg Kα radiation (h·ν=1253.6 eV). RT emission spectra were measured using a standard spectrofluorometer Edinburgh Instruments FLSP920 (Edimburgh, Scotland, UK), equipped with a 450W Xe lamp excitation source, at an excitation wavelength of 365 nm. EXAFS measurements of titania samples were carried out at Spanish CRG BM25A SpLine beamline (REF-A) at ESRF (The European Synchrotron Radiation Facility, Grenoble, France) [38]. X-ray absorption data were collected around Ti K-edge using a -70 °C ethanol cooled double Si(111) crystal, which gives an energy resolution of $\Delta E/E = 1.5x10^{-4}$. The experiment was performed at room temperature in fluorescence mode at standard 45° geometry. For fluorescence detection, Sirius liquid nitrogen cooled multi-element solid state X-Ray detector from e2v was employed. The detector includes 13 Si(Li) crystal sensors mounted on a low noise electrically restored FETs. Pure commercial TiO_2 anatase (Aldrich), the nitrogen-doped and the oxygen-rich samples were measured in the energy range from 4.8 to 5.7 keV.

Demeter package software was used for data processing[39]. Background removal and Tröger self-absorption correction in the raw data were carried out using Athena software[40]. Artemis software was used to complete the EXAFS data analysis. Pure commercial TiO_2 anatase sample data were used to build the structural model. Two coordination shells around central Ti atoms were fitted in the range from 1.4 to 3.5 Å.

Photocatalytic reaction. The photocatalytic properties of the prepared materials were evaluated in the reactions of photodegradation and partial photooxidation using *p*-cresol HMF as model compounds, respectively. The tests were carried out in aqueous phase in a stirred batch pyrex reactor containing 1 g L^{-1} of the photocatalysts suspended in 100 mL of the substrate

solutions. The light source was a 500 W lamp (Helios Italquartz) with emission maximum at 365 nm and equipped with a water-cooling jacket and positioned at a distance of 10 cm from the reaction vessel. The selected photocatalytic runs were carried out using a UV-cutoff filter solution of $NaNO_2$ (2 M). The optimum quantity of the photocatalysts was established based on the radiometric studies, and it ensures almost complete light absorption for all the samples. Before the radiation started the photocatalysts were suspended in the reaction solution with an assistance of ultrasonication and then mixed in the dark for 30 min, in order to complete the adsorption-desorption equilibrium. The concentrations of the substrates were 10 mg L^{-1} (0.093 mM) for *p*-cresol, as a pollutant, which is normally found in water at low concentration levels, and 40 mg L^{-1} (0.32 mM), 200 mg L^{-1} (1.6 mM), and 400 mg L^{-1} (3.2 mM) for HMF. The aliquots of approximately 2.5 mL were withdrawn from the reactor at the fixed time intervals, filtered through a PTFE 0.2 μm filter, and the concentrations of all compounds of interest extracted from water solutions in ethyl acetate were determined using a Shimadzu 2100 Ultra GC-MS system equipped with a Teknokroma TRB-5MS (95%) dimethyl (5%) diphenylpolysiloxane copolymer column. The analysis was carried out in a split regime, the injection port was at 250 ºC, the initial column temperature was 60 ºC, then the column was heated at 15 ºC·min^{-1} up to 180 ºC, then the temperature increased to 270 ºC at a rate of 40 ºC·min^{-1} and left for 2 min. Prior to each analytical run GC-MS system was calibrated for *p*-cresol or for HMF and FDC depending on the type of the reaction.

3. RESULTS AND DISCUSSION

3.1 Structural features of N-doped and oxygen-rich titania. The phase composition of the titania prepared by the described procedure and treated in a wide temperature range was already

described elsewhere[26]. Only pure anatase phase is detected for all the studied temperatures (Fig. 1). High crystallinity of the TiO_2 is confirmed by the amorphous content estimation, which changes only slightly as the calcination conditions change, reaching its maximum value at the highest thermal treatment temperature (Table 1). The unit cell parameters show significant discrepancies, especially the *c* dimension of the anatase unit cell, which grows along with increasing of the annealing temperature of the samples. This parameter exceeds that of pure commercial titania for T_600 and T_800 samples indicating the existence of certain structural perturbations (Table 1).

Considering that the precursors for the TiO_2 samples contain the sources of sulphur and nitrogen, one might attribute the changes of the anatase crystallographic parameters to the effect of non-metal doping, especially taking into account the bright yellow colour of the samples calcined at 400 and 500 ^oC. Indeed, the sulphur is not detected by any of the used analytical methods (XPS, EELS, and CHNS-analysis), while the presence of nitrogen is obvious from the EELS data. The nitrogen content appears to be relatively high for T_400 and T_500, but it is completely removed at higher temperatures (Fig. 2, Table 1). Earlier, we observed that no nitrogen was found for the same type of TiO_2 treated at 800 ^oC[26]. We suppose that the application of NH_4OH for the pH adjustment of the titanium hydroxide suspension in the work of Etacheri *et al* might had led to the nitrogen incorporation into the TiO_2 structure, as in the present case, although the characterization of the materials prepared at temperatures below 600 ^oC was not reported[12].

Contrary to the supposition expressed in[12], we consider the N-doping, not the oxygen gas released from the decomposed peroxo complex precursor during the thermal treatment, as absolutely crucial for the following development of oxygen-rich TiO_2 under higher temperatures.

It was demonstrated in numerous works, that the peroxo species in the titanium peroxo complexes were decomposed at temperatures not higher than 300 ^{o}C[41-44], consequently the oxygen gas released by this reaction cannot affect the formation of TiO_2 structure at largely higher temperatures. Moreover, considering that pure TiO_2 is a stable compound in the studied temperature range, where Ti has a perfectly satisfying 6-coordinated state and exists in its highest oxidation state, there is no thermodynamic force, which would induce the incorporation of super stoichiometric oxygen into the crystal network. On the other hand, the crystal defects created by the incorporation of dopants or impurities might provoke the formation of oxygen vacancies causing a charge imbalance in the TiO_2 cell, which would tend to be compensated by the reduction of Ti^{4+} to Ti^{3+}, Ti^{2+} or by trapping oxygen from the atmosphere, which would occupy the vacant sites. Although, the role of nitrogen doping and its effect on the titanium local arrangement, in our view, is crucial for the preparation of oxygen-rich TiO_2, the importance of hydrogen peroxide concentration in the synthesis of this material must not be underestimated. In our opinion, high concentration of H_2O_2 provides the titanium complexation by the peroxo ligands and stabilization of the ammonium peroxotitanate, thus facilitating the incorporation of nitrogen species into the TiO_2 under thermal treatment.

The electronic structure of the titania materials was studied by UV-vis spectroscopy and by measuring the valence band (VB) potential by XPS. The DR UV-vis study clearly demonstrates the effect of the nitrogen-doping on the electronic properties of T_400 and T_500 samples, as the light-absorbance is extended to the visible-light region and the BG values are estimated to be 3.05 and 3.10 eV respectively (Fig. 3(A), (B)). Nitrogen impurities induce sub-bandgap states resulting in the appearance of the second absorption edge at about 2.3 eV observed for T_400 and T_500 (Fig. 3 (A), (B), Table 1), similar effect of N-doping was also reported by Bellardita

et al[45]. The elimination of nitrogen species, capable of reducing the titania bandgap, leaves its position almost unchanged, while the sub-bandgap states and the corresponding visible-light absorption disappear completely (Fig. 3 (C), (D), Table 1).

Comentario [Office2]: Question 11

Comentario [Office3]: Question 6

From **Figure 4** is seen that both the N-doped and the N-free TiO_2 samples possess identical VB potential of 2.4 eV, thus the subtraction of BG from the VB potential gives us a conduction band (CB) value similar for all the studied TiO_2 materials and close to - 0.7 eV. Such a minor difference in the electronic structure of the N-doped titania from the pristine TiO_2 anatase, having BG, VB and CB values of 3.2, 2.5, and -0.7 eV respectively, indicates that the principal role of the N-doping is sensitizing for visible-light activation of the photocatalysts and it is related to the appearance of the sub-band-gap states in T_400 and T_500.

It is still not clear if only substitutional nitrogen species are able to shift the absorption edge of TiO_2 to the visible region, while the interstitial nitrogen dopants form interband states, which do not contribute to the visible-light activity of TiO_2 anatase[27]. Nonetheless, not only the Ti-N, Ti-N-O or Ti-O-N linkages should be considered as responsible for the visible-light activation, as oxygen vacancies and Ti^{3+} containing sites in doped titania, which formation might be as well provoked by the nitrogen interstitials, affect the susceptibility of the photocatalyst to certain radiation wavelengths[46]. Spectroscopic techniques allow establishing a state in which the nitrogen species are found in the TiO_2 structure. The FTIR spectrum of the as-prepared dried titanium peroxo complex precursor (Fig. 5) shows the presence of O-O bonds vibration at 889 cm^{-1}, adsorbed and chemically bonded water manifesting itself by the bands at 3380 and 1630 cm^{-1}, but most importantly the presence of absorption at 1431 cm^{-1} and several bands between 2800 and 3200 cm^{-1} assigned to the N-H vibrations and attributed to the NH_4^+ of the dried ammonium peroxotitanate complex or adsorbed ammonium cation. The same observations were

also made by Etacheri *et al* studying FTIR data of the precursor[12]. Thermal treatment of the precursor in air at 250 ^{o}C for 2 h resulted in a complete elimination of peroxo groups and significant reduction of quantity of bonded NH_4^+, instead another absorption band at 1286 cm^{-1} appears (Fig. 5). Hadjiivanov *et al* pointed out that the band found at the same position is attributed to N-O vibration of various TiO_2-NO_2 surface complexes[47]. Thus, we suppose that the ammonium cations of the precursor react with the oxygen of TiO_2 lattice forming N-O species, which under crystallization are incorporated into the titania structure upon crystallization. The FTIR spectra registered for the samples calcined at higher temperatures do not show any valuable features due to low concentration of dopants residing in the titanium dioxide.

The presence of the nitrogen species in the TiO_2 was also probed by XPS, however nitrogen was only detected in T_400 sample, while the concentration of it in T_500 was below the detection limit (See Supplementary Information Fig. S1). Even more valuable than elemental analysis is the information about state of the atomic components of these samples obtained from XPS data. The signal coming from Ti $2p_{3/2}$ contains two major contributions Ti-1 located at 458.9 eV and Ti-2 having a maximum at 460.2 eV, both of which have reasonable half-width half-maximum (HWHM) values of about 0.8-0.9 eV for the N-doped (Fig. 6 (A), (B)) as well as for the N-free samples (Fig. 6 (C), (D)). Ti-1 peak is undoubtedly attributed to the octahedrally coordinated titanium of the TiO_2 crystalline network, while the second contribution might be assigned to the bulk and surface TiO_x species with a distinct coordination number or chemical bonding. Indeed, many studies on titania-containing mixed oxide systems assign the peak shift of Ti $2p_{3/2}$ to higher energies to the changes of Ti coordination from octahedral to tetrahedral[48-50]. The Ti-1 to Ti-2 peak ratio reveals a higher content of the Ti-species having a different coordination in the N-doped TiO_2 samples namely T_400 and T_500 compared to the nitrogen-

free ones (Table 2). Thus, the incorporation of nitrogen in titania affects the titanium coordination, leading to some distorted TiO_x units. Further heat treatment leads to a predominant contribution of Ti signal of the crystalline TiO_2 anatase, thus reducing the amount of the defect-sites containing Ti-species with Ti coordination number below 6 (Fig. 6 (C), (D) and Table 2).

Quantitative analysis of the chemical composition of the prepared materials by XPS revealed that the oxygen content increases with the temperature of the treatment (Table 2). This is most likely an indication of atmospheric O_2 capture by TiO_2. The O 1s XPS spectrum of TiO_2 usually contains two major contributions corresponding to lattice oxygen and adsorbed hydroxyl groups. However, in the present case the deconvolution of O 1s band into two components (not shown) yields large HWHM values for the peaks. That is why the spectra have been fitted to three contributions centred at 530.2 (O-1), at 531.8 eV (O-2) and 533.0 eV (O-3). The dominant peak at 530.2 eV (O-1) is assigned to the oxygen atoms of the TiO_2 crystalline network, the second one at 531.8 eV (O-2) corresponds to the oxygen of surface hydroxyl groups, and the third one at 533.0 eV (O-3) might be attributed to the contributions from adsorbed H_2O and chemisorbed oxygen species including those taking the form of peroxo groups[51-53]. The most heavily N-doped T_400 sample shows the highest ratio of O-1 to the sum of O-2 and O-3 indicating that oxygen in this material is mostly a part of the crystalline anatase TiO_2 (Fig. 7 (A), Table 2). When the thermally driven elimination of the nitrogen species starts at higher temperature, we observe a drastic change in O-2 and O-3 contributions to the O 1s spectrum of T_500 sample (Fig. 7 (B)). It is worth mentioning that, among all the samples, the highest relative content of disordered Ti-species and the lowest O-1 to O-2 and O-3 ratio are observed for T_500. This can be explained by the elimination of a large quantity of the N-dopants, which results in the creation of bulk defect-sites. On the other hand, the replacement of the N-containing surface sites with the surface

oxygens promotes higher titania hydroxylation. It is a common notion that titanium dioxide loses its surface hydroxyl groups and adsorbed H_2O while thermally treated, which would lead to a predominance of the O-1 component[54]. Here, on the contrary, we see that the area of O-2 barely decreases for the samples T_600 (Fig. 7(C)) and T_800 (Fig. 7(D)) in respect to the nitrogen-doped TiO_2 (Table 2), which means that some other than surface hydroxyls oxygen-containing species are formed in the TiO_2 after the N-dopants are removed at higher calcination temperatures. Furthermore, O-3 peak area even experiences an increase, which suggests that the increase in chemisorbed oxygen[51] or peroxo groups[52,53] compensates for the loss of absorbed H_2O.

Comentario [Office4]: Question 3 and Question 10

XAS, contrary to surface sensitive XPS, allows obtaining information on the oxidation state and the local order of Ti atoms from the bulk of TiO_2 materials, thus revealing the distortions caused by the incorporation of dopants or formation of other types of defects. If the defect-inducing species are present in the titanium dioxide at very low concentration levels, and hence they have only a minor effect on the long-range order of the TiO_2, many laboratory-scale instruments are unable to characterize the Ti local arrangement in-depth.

It may occur that N-doping provokes a partial reduction of Ti^{4+} to Ti^{3+} through the formation of O-vacancies and the charge-compensation effect. The XANES spectra of four samples show the same shape and the energy edge as the TiO_2 (Ti^{4+}) anatase reference (Fig. S2), thus indicating the absence of significant quantities of the reduced species, which is in accordance with the previously discussed XPS data.

EXAFS data analysis was carried out in order to determine the position of the dopants in the titania samples using a similar approach to that reported by Sahoo *et al*[32]. Crystallographic data for TiO_2 anatase reference phase was used to construct the model for fitting the spectra. Two

coordination shells around central Ti atom were fitted in the range from 1.4 to 3.5 Å and in the k-range of the Fourier transform from 2.6 to 11.8 $Å^{-1}$. Three main single scattering paths were used: Ti-O_{ax}, Ti-O_{eq} and Ti-Ti. In addition, several double scattering paths (Reff < 3.5 Å) were taken into account, using a combination of parameters from single scattering path in order to avoid exceeding of the limit of number of free variables determined by Nyquist theorem.

One can clearly observe the differences on the spectra of the N-TiO_2 after treatment at high temperatures (Fig. 8). It is of special importance that the shoulder present on the spectrum of T_400 is gradually replaced by another maximum manifesting itself on the spectra of T_600 and T_800 samples (Fig. 8). Although the shoulder seen for T_400 is not the signal directly coming from the N atoms, we attribute it to the redistribution of defects and displacement of oxygens neighbouring to the central Ti atom probably caused by the incorporation of nitrogen-dopants. Thus, the Ti-nitrogen interstitials (Ti-N_{int}) and Ti-oxygen interstitials (Ti-O_{int}) paths were included in the fit aiming to assess the influence of the dopants on the local order in the titania material. For the sake of comparison, the commercial TiO_2 anatase powder of 99 % purity was measured and fitted in order to calculate S02 and ΔE0 values to be further used in the fitting model. **Figure 9** displays the quality of the EXAFS spectra fitting. It is clear that a good fit is obtained for the first two coordination shells of Ti.

The highest concentration of nitrogen provokes the reduction of the coordination number Ti—O in the first coordination shell in respect to the commercial TiO_2 anatase, which is the consequence of the N-species incorporation both by axial and equatorial positions (Table 3). The N-doping in the case of T_400 barely affects the Ti-O bond distance resulting it to be almost the same as in the reference material, where $(Ti–O)_{eq}$ and $(Ti–O)_{ax}$ distances are 1.94 and 1.98 Å equal to those calculated by Ceotto e*t al* for the pristine titania[31]. The doping certainly influences

Comentario [Office5]: Question 2 and Question 9

Comentario [Office6]: Question 4

the TiO_2 microstructure by causing the formation of oxygen vacancies in the first coordination shell and creation of doping sites at a larger distance from the central atom (Fig. S3 (A), Table 3). The fitting of the Ti-N_{int} path to the model shows that the distance between the central atom and the N-species is about 2.4 Å, which is in agreement with the axially positioned Ti-N_{int} distance calculated by Ceotto *et al* using DFT method[31]. The coordination number of Ti-N_{int} is calculated to be nearly 1, which sums with oxygens bonded to the titanium atom giving the Ti coordination number of 6, thus satisfying its octahedral arrangement (Table 3). However, giving low concentrations of nitrogen found in the studied material, one must not think that this path included in the fit demonstrates the existence of titanium nitride bonds neither does it imply that every sixth O atom in the vicinity of the Ti is replaced by one N. As nitrogen and oxygen atoms are indistinguishable by the applied analytical technique due to their very similar electron density, it is rather an indication of the presence of NO_x species at a certain distance from Ti in the TiO_2 network. Moreover, according to the XPS study, nitrogen is present in the material in the oxidized form (Fig. S1), so it is most likely that the doping of the TiO_2 occurs by the incorporation of the N-interstitials forming in this way the Ti-O-N bonds (Fig. 10 (A), (B)). The increase of the calcination temperature under air atmosphere causes the part of nitrogen to be eliminated from the titania (Table 1, Fig. 2). The N-dopants are evolved in the form of NO, thus leaving the vacancies in the TiO_2 network and provoking a charge imbalance, which is in accordance with the XPS study demonstrating the largest quantity of the disordered TiO_x sites in T_500 among the all samples (Fig. 6 (B), Table 2). According to the mechanism of oxygen interstitials formation in titanium dioxide doped with Nb ions proposed in[22], the net-charge imbalance forces atmospheric oxygen to be adsorbed on the titania surface and then slowly diffuses to the vacant sites, as to TiO_6 polyhedral units recover their charge neutrality. For T_500

Comentario [Office7]: Question 2 and Question 9

Comentario [Office8]: Question 4

Comentario [Office9]: Question2 and Question 9

we can clearly see a new contribution at a distance of 2.6 Å, which we attribute to the interstitial oxygen species (Table 3). Also, the equatorial Ti-O bonds result to be influenced by the incorporation of O as the distance is significantly increased (Fig. S3 (B), Table 3). All nitrogen dopants are removed by the thermal treatment at 600 ^{o}C and totally replaced by oxygen interstitials (Fig. 8, Fig. 10 (C)). The distance of Ti-O_{int} in this sample is maintained almost the same as in T_500, while the Ti-O equatorial bond length reaches its highest value (Fig. S3 (B), Table 3). This observation is in accordance with the earlier described elongation of the crystallographic *c*-parameter and the expansion of the titania anatase unit cell (Table 1), as well as with the computation data presented by Lo Presti *et al*[55], where interstitial N-dopants had the similar effect on the TiO_2 crystal structure. It is important to mention that at this point the sum of Ti-O_{eq}, Ti-O_{ax}, Ti-O_{int} coordination numbers gives a value superior that of the reference anatase TiO_2 (Table 3). It is known that titanium atom acquires a coordination number of 7 in peroxo complexes[56], and the formation of O_2^{2-} (peroxo), O_2^{-} (superoxo) along with bridging dimer $(O_2)_o$ species in oxygen-rich titania (Fig. 10 (C)) was as-well proposed in the study[22]. In accordance with this, XPS study, discussed above, shows the contribution at 533 eV on the 1s O spectra also suggesting the presence of some chemisorbed oxygen species or peroxo groups (Table 2). Peroxo groups coordinated to titanium are able to absorb the visible-light, which is most likely a cause of a slight BG shrinkage in respect to the pristine TiO_2 anatase (Table 1). The further increase of the calcination temperature almost completes the process of occupation of defect sites produced by the N-species elimination, as the coordination number of Ti to the neighbouring oxygens in T_800 is back to 6 (Fig. S3 (A), Table 3). The Ti-O_{eq} bond length decreases compared to that of T_600 sample indicating that the O_2 adsorption process is probably completed and the internal rearrangement inside the TiO_2 cell is taking place. In our previous work[26] we found out that the

Comentario [Office10]: Question 11

Comentario [Office11]: Question 3 and Question 10

calcination of this material at temperatures superior 800 ^{o}C causes it to partially transform to rutile phase, this is why this study is limited to the 400-800 ^{o}C range, as to avoid the application of another crystallographic phase to be included in the model making it less precise.

3.2 Photocatalytic properties of N-doped and oxygen-rich titania

3.2.1 Photocatalytic degradation of *p*-cresol. All the studied materials are active in the UV-vis assisted decomposition of *p*-cresol. The N-doped samples T_400 and T_500 show intermediate activity totally degrading the pollutant after 240 and 210 min of the reaction respectively (Fig. 11 (A)). The thermal treatment of TiO_2 at 600 ^{o}C results in a complete elimination of the N-dopants producing the most active photocatalyst (Fig. 11 (A)). Up to this point the activity increases despite the reduction of SSA values (Table 1). To explain this slight increase of the reaction rate after the removal of N-dopants one might address to the PL spectra of the two most representative of the series T_400 and T_600 samples, where it is clearly seen that the recombination rate is reduced for the oxygen-rich TiO_2 samples (Fig. S4). Thus, the N-species or the oxygen vacancies in the first coordination shell formed in the result of N incorporation in TiO_2 play role of recombination centers, while the O-doping by filing the vacant sites in the Ti environment (Table 3) and producing O-interstitial does not hinder the charge transfer. Further increase of the treatment temperature leads to the sintering of the TiO_2[26] and diminishing of SSA value. This results in that T_800 demonstrates the worst photocatalytic performance of the present samples (Fig. 11 (A)).

By cutting off the UV irradiation we intended to verify the effect of the N- and O-dopants on the visible-light activation of the titania photocatalysts. Sample T_400 containing the highest concentration of the nitrogen species is the most active under the visible-light (Fig. 11 (B)).

Lower nitrogen content of T_500 sample reduces the utilization of the visible-light irradiation, hence some reduction of the *p*-cresol photodegradation rate is observed (Fig. 11 (B)). Contrary to the UV-vis assisted photocatalytic study, the removal of the N-species is detrimental for the photocatalytic performance of T_600, as it loses a lot of the visible-light susceptibility (Fig. 11 (B)). Not surprisingly the further enhancement of the calcination temperature reduces the photoactivity even more (Fig. 11 (B)). However, even if the N-dopants are completely removed, the TiO_2 samples maintain the visible-light assisted photocatalytic activity indicating on the important role of the oxygen interstitials of oxygen-rich titania in the sensitization of the photocatalyst.

3.2.2 Partial photooxidation of HMF to FDC. Almost all of the studied TiO_2 samples demonstrate very similar trends of HMF conversion with an exception of T_800, which is significantly less active due to its low SSA (Fig. 12 (A)). As in the case of the p-cresol degradation, the slight increase of the reaction rate observed for the samples treated at temperatures of 500 and 600 ^{o}C compared to that of T_400, which is most likely to be attributed to the decreased recombination rate associated to the nitrogen removal (Fig. S4). However, the reaction does not go exactly the same way for the N- and O-doped photocatalysts. The photooxidation of HMF in the presence of the N-doped TiO_2 compared to the N-free titania samples gives higher quantities of a valuable partial oxidation product FDC (Fig. 12 (B)), which might be formed in the result of a hydrogen abstraction from the OH group of HMF by photogenerated holes or $^{\bullet}O_2^-$ radicals[57,58]. Although, relatively high concentrations of FDC are observed during the photocatalytic runs, one should mention a certain decline of the selectivity values with the reaction time (Fig. 12 (C)). From **Figure 12 (D)** it is clear that the N-doped TiO_2

samples have higher selectivity values than that of the oxygen-rich titania at the same conversion degrees. The descending character of the selectivity curve with time is improved if higher concentrations of the substrate are used. Selectivities to FDC oxidation of about 30-40 % are reached when T_400 is used as photocatalysts at HMF concentrations of 1.6 and 3.2 mM (Fig. S5).

A partial photocatalytic oxidation of alcohols in general and HMF in particular might be promoted by the reaction with O_2^- radicals generated *via* oxygen reduction pathway on semiconductor photocatalysts such as g-C_3N_4, which is unable to form $OH^\bullet$ radicals by the direct interaction of positively charged holes with water[58]. Titanium dioxide, on the other hand, possesses a VB potential favourable to $^\bullet$OH formation, hence only very disordered TiO_2 materials with high content of amorphous phase are usually applied for partial photooxidation reactions with an intention to supress $^\bullet$OH generation[34,59]. High concentration of various surface and bulk defects in poorly crystalline material makes difficult assessing the influence of nitrogen-doping on selective photooxidation performance of titanium dioxide, although such attempt was made[34], that is why it is of special interest to compare well-crystalline N-TiO_2 and oxygen-rich TiO_2 anatase in this type of reactions. From the presented data it is clear that N-doping favours partial oxidation of HMF to FDC, while oxygen-rich titania is obviously more efficiently performs in photodegradation of the water pollutants. Considering the fact that both types of TiO_2 samples possess nearly the same electronic structure (Fig. 3, 4), which are responsible for the generation of electron-hole pairs, we find the explanation of their very different photocatalytic behaviour in the modification of the surface active sites. It was mentioned in Section 3.1 that ammonia containing in the precursor material reacts with Ti-O sites forming Ti-O-N linkages, thus leaving the surface poor in hydroxyl groups, which was

confirmed by the XPS study (Fig. 7 (A), Table 2). This has a twofold effect: first, it inhibits the generation of $OH^{\bullet}$ radicals on the titania surface and it complicates the interaction of the surface sites with the reaction products, thus reducing the decomposition of FDC. It results that the selectivity values of HMF to FDC conversion obtained for the well-crystalline N-TiO_2 are closed to those reported for the poorly crystalline titania and superior than that of the commercial titanium dioxide[59].

CONCLUSIONS

Titanium local structure study has allowed us reconsidering the mechanism of oxygen-rich titania formation from a precursor containing a source of nitrogen. We have demonstrated that at low temperatures of thermal treatment (400-500 ^{o}C) nitrogen-doping of TiO_2 anatase titania occurs, and the N-species occupy interstitial position in the titanium dioxide anatase crystal structure causing creation of defects (oxygen vacancies) in the titanium first coordination shell. The treatment under air at high temperatures completely removes the N-dopants, thus leaving the Ti coordination unsatisfied provoking the charge imbalance in the TiO_5 units. It forces the neighbouring oxygen atoms to occupy a vacant place, which in its turn results in the cascade reaction of adsorption of atmospheric oxygen and its diffusion to the unoccupied sites. The captured oxygen forms the interstitial O-species inside the TiO_2 network, expanding the TiO_2 crystal cell. The coordination number of Ti in the oxygen-rich titania exceeds the value of 6, thus implying the formation of O-O peroxo bridges coordinating titanium atoms.

Both types of the dopants affect in the similar way the electronic properties of TiO_2 slightly reducing its BG value by shifting the VB to 2.4 eV. Despite the fact that all the samples are active under the wavelengths of ≥400 nm, the interband state formed by the N-species

incorporation provides better sensitization of photocatalyst than the O-dopants do, thus permitting more efficient visible-light utilization. On the basis of the photocatalytic studies, we have also suggested that the N-doping and the oxygen vacancies it produces in the first coordination shell of Ti might be responsible for the reduced photocatalytic reaction rate in the case of p-cresol degradation as well as in HMF photoconversion. On the other hand, the presence of the N-species on the titania modifies its surface chemistry reducing the hydroxylation degree making it the most probable contributing factor to a higher selectivity of N-TiO_2 in the photooxidation of HMF to FDC by hindering the transfer of the unselective •OH radicals from the catalyst surface to the substrate and the product molecules. Thus, the presented investigation does not only shed the light on the question of formation of oxygen-rich TiO_2, but also it demonstrates the importance of a rational design of doped titania materials for the application in different types of photocatalytic reactions.

ASSOCIATED CONTENT

Supporting Information. XPS, XANES and photoreactivity data. This material is available free of charge via the Internet at http://pubs.acs.org.

Corresponding Author. Igor Krivtsov. E-mail: uo247495@uniovi.es; zapasoul@gmail.com, tel. +34 684348116, 33006, Julian Claveria 8, Oviedo, Spain

ACKNOWLEDGMENT

This work was financially supported by Spanish MINECO (MAT2013-40950-R, MAT2016-78155-C2-1-R, and CTQ2014-52956-C3-1-R), Gobierno del Principado de Asturias (GRUPIN14-060 and GRUPIN14-078), FEDER and South Ural State University thanks for the support the Ministry of Education and Science of the Russian Federation (grant No

16.2674.2014/K). IK acknowledges the support by Act 211 Government of the Russian Federation, contract № 02.A03.21.0011.

REFERENCES

(1) Chen, X.; Mao, S.S. Titanium dioxide nanomaterials: Synthesis, properties, modifications, and applications. *Chem. Rev.* **2007**, 107, 2891–2959.

(2) Hun, F.; Kambala, V.S.R.; Srinivasan, M.; Rajarathnam, D.; Naidu, R. Tailored titanium dioxide photocatalysts for the degradation of organic dyes in wastewater treatment: A review. *Appl. Catal. A: General.* **2009**, 359, 25-40.

(3) Ma, Y.; Wang, X.; Jia, Y.; Chen, X.; Han, H.; Li, C. Titanium dioxide-based nanomaterials for photocatalytic fuel generations. *Chem Rev.* **2014**, 114, 9987-10043.

(4) Gaya, U.I.; Abdullah, A.H. Heterogeneous photocatalytic degradation of organic contaminants over titanium dioxide: A review of fundamentals, progress and problems. *J. Photochem. Photobiol. C: Photochem. Rev.* **2008**, 9, 1-12.

(5) Pelaez, M.; Nolan, N.T.; Pillai, S.C.; Seery, M.K.; Falaras, P.; Kontos, A.G.; Dunlop, P.S.M.; Hamilton, J.W.J.; Byrne, J.A.; O'Shea, K. *et al*. A review on the visible light active titanium dioxide photocatalysts for environmental applications. *Appl. Catal. B: Environ.* **2012**, 125, 331-349.

(6) Etacheri, V.; Valentin, C.D.; Schneider, J.; Bahnemann, D.; Pillai, S.C. Visible-light activation of TiO_2 photocatalysts: Advances in theory and experiments. *J. Photochem. Photobiol. C: Photochem. Rev.* **2015**, 25, 1-29.

(7) Wang, Y.; Wang, Q.; Zhan, X.; Wang, F.; Safdar, M.; He, J. Visible light driven type II heterostructures and their enhanced photocatalysis properties: a review. *Nanoscale*, **2013**, 5, 8326-8339.

(8) Rehman, S.; Ullah, R.; Butt, A.M.; Gohar, N.D. Strategies of making TiO_2 and ZnO visible light active. *J. Hazard. Mater.* **2009**, 170, 560-569.

[9] Asahi, R.; Morikawa, T.; Irie, H.; Ohwaki, T. Nitrogen-doped titanium dioxide as visible-light-sensitive photocatalyst: Designs, developments, and prospects. *Chem. Rev.* **2014**, 114, 9824−9852.

(10) Nakamura, I.; Negishi, N.; Kutsuna, S.; Ihara, T.; Sugihara, S.; Takeuchi, K. Role of oxygen vacancy in the plasma-treated TiO_2 photocatalyst with visible light activity for NO removal. *J. Molecul. Catal. A: Chem.* **2000**, 161, 205-212.

(11) Kong, X.; Zeng, C.; Wang, X.; Huang, J.; Li, C.; Fei, J.; Li, J.; Feng, Q. Ti-O-O coordination bond caused visible light photocatalytic property of layered titanium oxide. *Sci. Report.* **2016**, 6, 29049.

(12) Etacheri, V.; Seery, M.K.; Hinder, S.J.; Pillai, S.C. Oxygen Rich Titania: A dopant free, high temperature stable, and visible-light active anatase photocatalyst. *Adv. Funct. Mater.* **2011**, 21, 3744-3752.

(13) Mamontov, E.; Egami, T.; Brezny, R.; Koranne, M.; Tyagi, S. Lattice defects and oxygen storage capacity of nanocrystalline ceria and ceria-zirconia. *J. Phys. Chem. B.* **2000**, 104, 11110-11116.

(14) León-Reina, L.; Losilla, E.R.; Martínez-Lara, M.; Bruque, S.; Aranda, M.A.G. Interstitial oxygen conduction in lanthanum oxy-apatite electrolytes. *J. Mater. Chem.* **2004**, 14, 1142–1149.

(15) León-Reina, L.; Porras-Vazquez, J.M.; Losilla, E.R.; Aranda, M.A.G. Interstitial oxide positions in oxygen-excess oxy-apatites. *Solid State Ionics.* **2006**, 177, 1307–1315.

(16) Nakamura, T.; Ling, Y.; Amezawa, K. The effect of interstitial oxygen formation on the crystal lattice deformation in layered perovskite oxides for electrochemical devices. *J. Mater. Chem. A.* **2015**, 3, 10471–10479.

(17) Kamisaka, H.; Yamashita, K. Theoretical study of the interstitial oxygen atom in anatase and rutile TiO_2: electron trapping and elongation of the r(O_O) bond. *J. Phys. Chem. C.* **2011**, 115, 8265–8273.

(18) Li, Y.-F.; Aschauer, U.; Chen, J.; Selloni, A. Adsorption and reactions of O_2 on anatase TiO_2. *Acc. Chem. Res.* **2014**, 47, 3361−3368.

(19) Lee, H-Y.; Robertson, J. Doping and compensation in Nb-doped anatase and rutile TiO_2. *J. Appl. Phys.* **2013**, 113, 213706.

(20) Close, T.; Tulsyan, G.; Diaz, C.A.; Weinstein, S.J.; Richter, C. Reversible oxygen scavenging at room temperature using electrochemically reduced titanium oxide nanotubes. *Nature Nanotech.* **2015**, 10, 418–422.

(21) Hollister, A.G.; Gorai, P.; Seebauer, E.G. Surface-based manipulation of point defects in rutile TiO_2. *Appl. Phys. Lett.* **2013**, 102, 231601.

(22) Setvín, M.; Aschauer, U.; Scheiber, P.; Li, Y-F.; Hou, W.; Schmid, M.; Selloni, A.; Diebold, U. Reaction of O_2 with subsurface oxygen vacancies on TiO_2 anatase (101). *Science*. **2013**, 341, 988.

(23) Tan, L-L.; Ong, W-J.; Chai, S-P.; Mohamed, A.R. Visible-light-activated oxygen-rich TiO_2 as next generation photocatalyst: Importance of annealing temperature on the photoactivity toward reduction of carbon dioxide. *Chem. Eng. J.* **2016**, 283, 1254–1263.

(24) Tan, L-L.; Ong, W-J.; Chai, S-P.; Mohamed, A.R. Band gap engineered, oxygen-rich TiO_2 for visible light induced photocatalytic reduction of CO_2. *Chem. Commun.* **2014**, 50, 6923-6926.

(25) Tan, L-L.; Ong, W-J.; Chai, S-P.; Goh, B.T.; Mohamed, A.R. Visible-light-active oxygen-rich TiO_2 decorated 2D graphene oxide with enhanced photocatalytic activity toward carbon dioxide reduction. *Appl. Catal. B: Environ.* **2015**, 179, 160-170.

(26) Krivtsov, I.; Ilkaeva, M.; Avdin, V.; Amghouz, Z.; Khainakov, S.A.; García, J.R.; Díaz, E.; Ordóñez, S. Exceptional thermal stability of undoped anatase TiO_2 photocatalysts prepared by a solvent-exchange method. *RSC Adv*. **2015**, 5, 36634-36641.

(27) Di Valentin, C.; Finazzi, E.; Pacchioni, G.; Selloni, A.; Livraghi, S.; Paganini, M.C.; Giamello, E. N-doped TiO_2: Theory and experiment. *Chem. Phys.* **2007**, 339, 44-56.

(28) Chen, H.; Nambu, A.; Wen, W.; Graciani, J.; Zhong, Z.; Hanson, J.C.; Flujita, E.; Rodriguez, J.A. Reaction of NH_3 with titania: N-doping of the oxide and TiN formation. *J. Phys. Chem. C.* **2007**, 111, 1366-1372.

(29) Belver, C.; Bellod, R.; Stewart, S.J.; Requejo, F.G.; Fernández-García, M. Nitrogen-containing TiO_2 photocatalysts. Part 2. Photocatalytic behaviour under sunlight excitation. *Appl. Catal. B.: Environ.* **2006**, 65, 309-314.

(30) Belver, C.; Bellod, R.; Fuerte, A.; Fernández-García, M. Nitrogen-containing TiO_2 photocatalysts. Part 1. Synthesis and solid characterization. *Appl. Catal. B.: Environ.* **2006**, 65, 301-308.

(31) Ceotto, M.; Lo Presti, L.; Cappelletti, G.; Meroni, D.; Spadavecchia, F.; Zecca, R.; Leoni, M.; Scardi, P.; Bianchi, C.L.; Ardizzone, S. About the nitrogen location in nanocrystalline N-doped TiO_2: Combined DFT and EXAFS approach. *J. Phys. Chem. C.* **2012**, 116, 1764-1771.

(32) Sahoo, M.; Yadav, A.K.; Jha, S.N.; Bhattacharyya, D.; Mathews, T.; Sahoo, N.K.; Dash, S.; Tyagi, A.K. Nitrogen location and Ti-O bond distances in pristine and N-doped TiO_2 anatase thin films by X-ray absorption studies. *J. Phys. Chem. C.* **2015**, 119, 17640-17647.

(33) Ahmed, S.; Rasul, M.G.; Martens, N.W.; Brown, R.; Hashib, M.A. Heterogeneous photocatalytic degradation of phenols in wastewater: A review on current status and developments. *Desalination.* **2010**, 261, 3-18.

(34) S. Yurdakal, V. Augugliaro, V. Loddo, G. Palmisano, L. Palmisano. Enhancing selectivity in photocatalytic formation of p-anisaldehyde in aqueous suspension under solar light irradiation via TiO_2 N-doping. New J. Chem., 2012, 36, 1762–1768.

(35) Amarasekara, A.S.; Green, D.; Williams, L.D. Renewable resources based polymers: Synthesis and characterization of 2,5-diformylfuran-urea resin. *Eur. Polym. J.* **2009**, 45, 595-598.

(36) Hui, Z.; Gandini, A. Polymeric schiff bases bearing furan moieties. *Eur. Polym. J.* **1992**, 28, 1461-1469.

(37) Kanetaka, Y.; Yamazaki, S.; Kimura, K. Preparation of Poly(ether ketone)s derived from 2,5-Furandicarboxylic Acid by Polymerization in Ionic Liquid. *Macromol.* **2016**, 49, 1252-1258.

(38) Castro, G.R. Optical design of the general-purpose Spanish X-ray beamline for absorption and diffraction. *J. Synchrotron Rad.* **1998**, 5, 657-660.

(39) Ravel, B.; Newville M. ATHENA, ARTEMIS, HEPHAESTUS: data analysis for X-ray absorption spectroscopy using IFEFFIT. *J. Synchrotron Rad.* **2005**, 12, 537–541.

(40) Tröger, L.; Arvanitis, D.; Baberschke, K.; Michaelis, H.; Grimm, U.; Zschech, E. Full correction of the self-absorption in soft-fluorescence extended x-ray-absorption fine structure. *Phys. Rev. B.* **1992**, 46, 3283–3289.

(41) Ilkaeva, M.; Krivtsov, I.; Avdin, V.; Khainakov, S.A.; García, J.R. Comparative study of structural features and thermal behaviour of mixed silica-titania xerogels prepared via the peroxo method and the conventional co-precipitation technique. *Colloid. Interface Sci. A: Physicochem. Eng. Asp.* **2014**, 456, 120-128.

(42) Ichinose, H.; Terasaki, M.; Katsuki, H. Synthesis of peroxo-modified anatase sol from peroxo titanic acid solution. *J. Ceram. Soc. Jpn.* **1996**, 104, 715–718.

(43) Liu, Y.-J.; Aizawa, M.; Wang, Z.-M.; Hatori, H.; Uekawa, N.; Kanoh, H. Comparative examination of titania nanocrystals synthesized by peroxo titanic acid approach from different precursors. *J. Colloid Interface Sci.* **2008**, 322, 497–504.

(44) Gao, Y.; Masuda, Y.; Peng, Z.; Yonezawa, T.; Koumoto, K. Room temperature deposition of a TiO2 thin film from aqueous peroxotitanate solution. *J. Mater. Chem.* **2003**, 13, 608–613.

(45) Bellardita, M.; Addamo, M.; Di Paola, A.; Palmisano, L.; Venezia A.M. Preparation of N-doped TiO_2: characterization and photocatalytic performance under UV and visible light. *Phys. Chem. Chem. Phys.* **2009**, 11, 4084–4093.

(46) Chen, Y.; Cao, X.; Lin, B.; Gao, B. Origin of the visible-light photoactivity of NH_3-treated TiO_2: Effect of nitrogen doping and oxygen vacancies. *Appl. Surf. Sci.* **2013**, 264, 845-852.

(47) Hadjiivanov, K.; Bushev, V.; Kantcheva, V.; Klissunski, D. Infrared spectroscopy study of the species arising during NO_2 adsorption on TiO_2 (Anatase). *Langmuir*. **1994**, 10, 464-471.

(48) Stakheev, A.Yu.; Shpiro, E.S.; Apijok, J. XPS and XAES study of TiO_2-SiO_2 system. *J. Phys. Chem.* **1993**, 97, 5668-5672.

(49) Luan, Z.; Maes, E.M.; van der Heide, P.A.W.; Zhao, D.; Czernuszewicz, R.S.; Kevan, L. Incorporation of titanium into mesoporous silica molecular sieve SBA-15. *Chem. Mater.* **1999**, 11, 3680-3686.

(50) Blasco, T.; Camblor, T.A.; Corma, A.; Perez-Pariente, J. The state of Ti in titanoaluminosilicates isomorphous with zeolite .beta. *J. Am. Chem. Soc.* **1993**, 115, 11806-11813.

(51) Han, X-G.; He, H-Z.; Kuang, Q.; Zhou, X.; Zhang, X-H.; Xu, T.; Xie, Z-X.; Zheng, L-S. Controlling Morphologies and Tuning the Related Properties of Nano/Microstructured ZnO Crystallites. *J. Phys. Chem. C.* **2009**, 113, 584–589.

(52) Kong, L.; Wang, C.; Zheng, H.; Zhang, X.; Liu, Y. Defect-Induced Yellow Color in Nb-Doped TiO2 and Its Impact on Visible-Light Photocatalysis. *J. Phys. Chem. C.* **2015**, 119, 16623−16632.

(53) Kong, X.; Zeng, C.; Wang, X.; Huang, J.; Li, C.; Fei, J.; Li, J.; Feng, Q. Ti-O-O coordination bond caused visible light photocatalytic property of layered titanium oxide. *Sci Rep.* **2016**, 6, 29049.

(54) Zhu, J.; Yang, J.; Bian, Z-F.; Ren, J.; Liu, Y-M.; Cao, Y.; Li, H-X.; He, H-Y.; Fan, K-N. Nanocrystalline anatase TiO_2 photocatalysts prepared via a facile low temperature nonhydrolytic sol–gel reaction of $TiCl_4$ and benzyl alcohol. *Appl. Catal. B.: Environ.* **2007**, 76, 82-91.

(55) Lo Presti, L.; Ceotto, M.; Spadavecchia, F.; Cappelletti, G.; Meroni, D.; Acres, R.G.; Ardizzone, S. Role of the Nitrogen Source in Determining Structure and Morphology of N-Doped Nanocrystalline TiO_2. *J. Phys. Chem. C.* **2014**, 118, 4797−4807.

(56) Tomita, K.; Petrykin, V.; Kobayashi, M.; Shiro, M.; Yoshimura, M.; Kakihana, M. A water-soluble titanium complex for the selective synthesis of nanocrystalline brookite, rutile, and anatase by a hydrothermal method. *Angew. Chem. Int. Ed.* **2006**, 45, 2378-2381.

(57) Spasiano, D.; Rodriquez, L.P.P.; Olleros, J.C.; Malato, S.; Marotta, R.; Andreozzi, R. TiO_2/Cu(II) photocatalytic production of benzaldehyde from benzyl alcohol in solar pilot plant reactor, Appl. Catal. B. 2013, 136-137, 56-63.

(58) Krivtsov, I.; García-Lopez, E.I.; Marcì, G.; Palmisano, L.; Amghouz, Z.; García, J.R.; Ordoñez, S.; Díaz, E. Selective photocatalytic oxidation of 5-hydroxymethyl-2-furfural to 2,5-furandicarboxyaldehyde in aqueous suspension of g-C_3N_4. *Appl. Catal. B.: Environ.* **2017**, 204, 430-439.

(59) Yurdakal, S.; Tek, B.S.; Alagoz, O.; Augugliaro, V.; Loddo, V.; Palmisano, G.; Palmisano, L. Photocatalytic selective oxidation of 5‑(hydroxymethyl)-2-furaldehyde to 2,5-furandicarbaldehyde in water by using anatase, rutile, and brookite TiO_2 nanoparticles. *ACS Sustainable Chem. Eng.* **2013**, 1, 456−461.

Figure captions

Figure 1. PXRD patterns of the titania samples: (—) T_400, (—) T_500, (—) T_600, and (—) T_800.

Figure 2. N region of EELS spectra obtained for: (—) T_400, (—) T_500, (—) T_600.

Figure 3. Tauc-plot of DR UV-vis data obtained for (A) T_400, (B) T_500, (C) T_600, (D) T_800.

Figure 4. XPS VB spectra of (—) T_400, (—) T_500, (—) T_600, and (—) T_800.

Figure 5. FTIR spectra of the titania samples (—) titanium peroxo complex precursor, (—) titanium peroxo complex precursor treated at 250 ^{o}C, (—) T_400, (—) T_500, (—) T_600, and (—) T_800.

Figure 6. XPS spectra of Ti $2p_{3/2}$ region of (**A**) T_400, (**B**) T_500, (**C**) T_600, and (**D**) T_800.

Figure 7. XPS spectra of O 1s region of (**A**) T_400, (**B**) T_500, (**C**) T_600, and (**D**) T_800.

Figure 8. Extended region fitting using ARTEMIS in R-space for (—) T_400,(—) T_500, (—) T_600, and (—) T_800 samples.

Figure 9. Fitted magnitude of the k^2-weighted Ti K-edge EXAFS spectra (left) and the corresponding EXAFS Fourier transform (right) for (A) commercial TiO_2 anatase, (B) T_400, (C) T_500, (D) T_600, (E) T_800 samples

Figure 10. Schematic representation of the N- and O-interstitial formation in the TiO_2 structure.

Figure 11. Photocatalytic degradation of p-cresol in the presence of (—) T_400,(—) T_500, (—) T_600, and (—) T_800 samples under (A) UV-vis and (B) $NaNO_2$ filtered (>400 nm) irradiation.

Figure 12. Photocatalytic conversion of HMF to FDC in the presence of (—) T_400,(—) T_500, (—) T_600, and (—) T_800 samples at HMF concentration of 40 mg L^{-1} (0.32 mM).

Figures

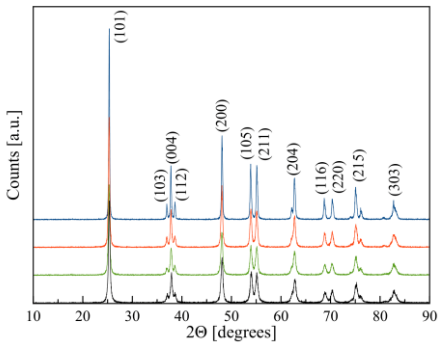

Fig. 1

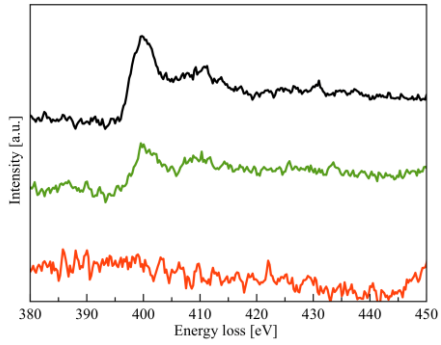

Fig. 2

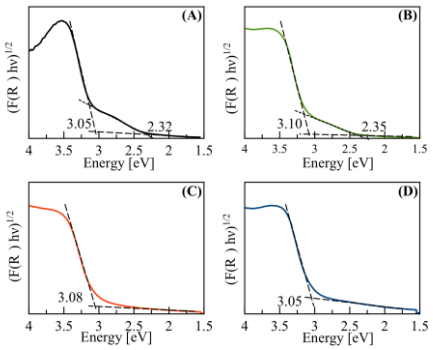
(A)
(B)
(C)
(D)
(F(R) hν)^1/2
Energy [eV]
3.05
2.32
3.10
2.35
3.08
3.05

Fig. 3

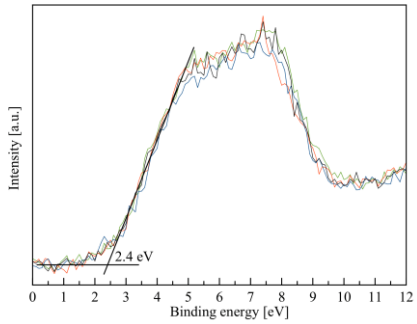
Intensity [a.u.]
2.4 eV
Binding energy [eV]

Fig. 4

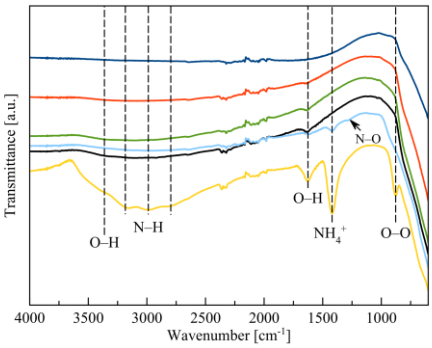
Transmittance [a.u.]
O–H
N–H
O–H
NH4+
N–O
O–O
Wavenumber [cm-1]

Fig. 5

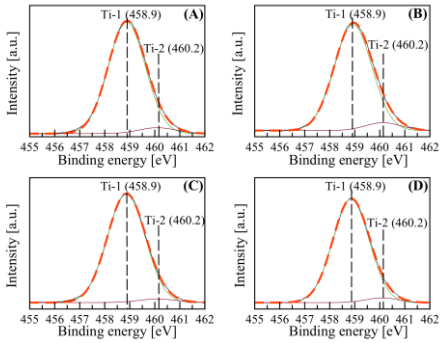

Fig. 6

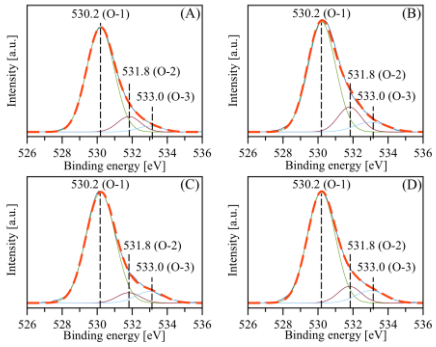

Fig. 7

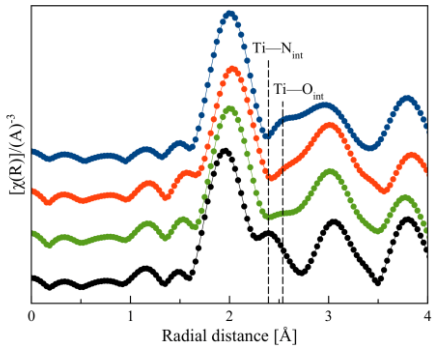
Ti—N$_{int}$
Ti—O$_{int}$
[χ(R)]/(A)$^{-3}$
Radial distance [Å]

Fig. 8

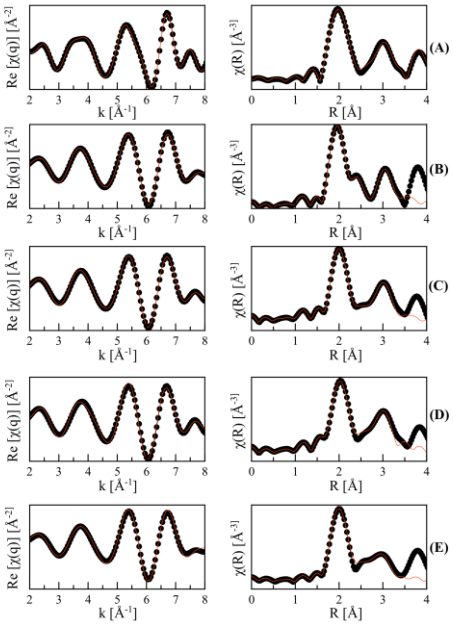
Re [χ(q)] [Å^{-2}]
k [Å^{-1}]
χ(R) [Å^{-3}]
R [Å]
(A)
(B)
(C)
(D)
(E)

Fig. 9

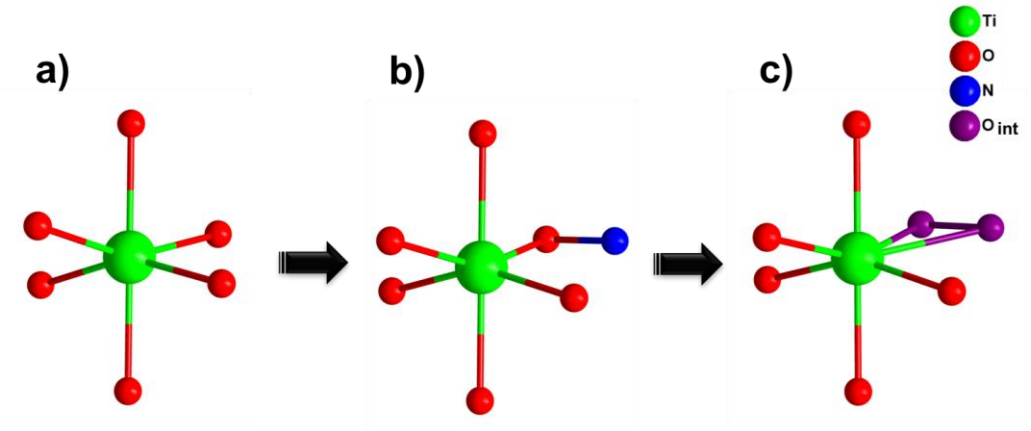

Fig. 10

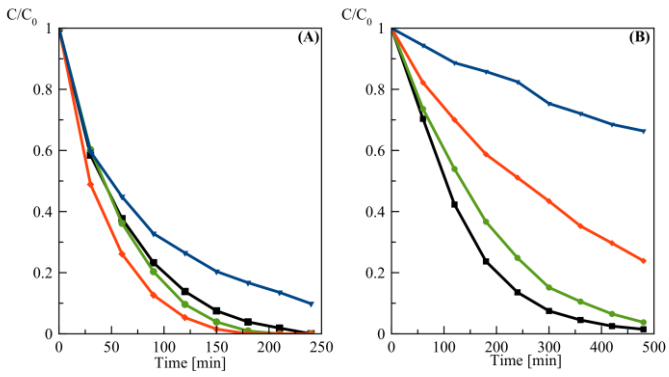

Fig. 11

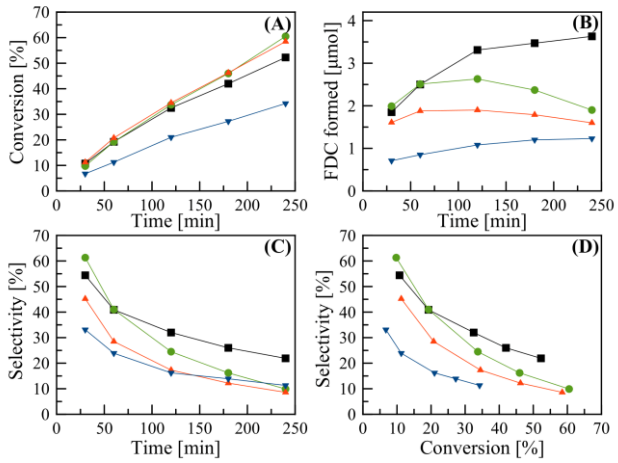
(A)
Conversion [%]
Time [min]
(B)
FDC formed [µmol]
Time [min]
(C)
Selectivity [%]
Time [min]
(D)
Selectivity [%]
Conversion [%]

Fig. 12

Tables

Table 1. Properties of the prepared titania samples

Sample	Crystal size [nm]	Unit cell parameters [Å]			Amorphous phase content [%]	Band gap [eV]	SSA [m^2g^{-1}]	EELS N [at%]	*K* [min^{-1}]
		a	c	Unit cell volume, [$Å^3$]					
T_400	22±1	3.7858(9)	9.5044(3)	136.22	3.4±0.4	3.05	81	6	0.0179
T_500	27±3	3.7848(7)	9.5084(3)	136.21	1.1±0.3	3.10	59	2	0.0223
T_600	33±3	3.7845(7)	9.5146(2)	136.27	2.5±0.3	3.08	36	0	0.0256
T_800	54±5	3.7833(5)	9.5245(2)	136.33	7.7±0.3	3.05	9	0	0.0101
Anatase (Aldrich)	91±7	3.7844(9)	9.5135(8)	136.25	0±0.1	3.20	5	0	

Table 2. XPS elemental composition (at. %) and deconvolution data

Comentario [Office12]: Question 3 and Question 10

Sample	Ti $2p_{3/2}$			O 1s				O/Ti ratio
	Ti-1, HWHM	Ti-2, HWHM	Ti-1/Ti-2 ratio	O-1, HWHM	O-2, HWHM	O-3, HWHM	O-1/O-2/O-3 ratio	
T_400	0.87	0.86	19	0.93	0.78	0.84	1/0.12/0.05	2.42
T_500	0.88	0.84	14	0.94	0.78	1.09	1/0.19/0.10	2.57
T_600	0.89	0.88	30	0.98	0.77	0.95	1/0.08/0.10	2.75
T_800	0.85	0.76	25	0.94	0.73	0.97	1/0.11/0.12	2.80

Table 3. The results of EXAFS data fitting.

Sample	Path	Coordination number	R [Å]	σ^2 [Å^2]
T_400	Ti-O equatorial	3.46 (2)	1.935 (2)	0.0003 (1)
	Ti-O axial	1.58 (2)	1.977 (2)	0.0003 (1)
	Ti-N_interstitial	0.99(6)	2.436 (4)	0.0004 (1)
	Ti-Ti	3.62 (2)	3.033 (1)	0.002 (1)
T_500	Ti-O equatorial	3.21 (2)	1.959 (2)	0.0003 (1)
	Ti-O axial	1.65(2)	1.975 (3)	0.0003 (1)
	Ti-N_interstitial	0.45(6)	2.352 (2)	0.0001 (1)
	Ti-O_interstitial	0.51(7)	2.581 (4)	0.002 (1)
	Ti-Ti	4.26(2)	3.035 (1)	0.002 (1)
T_600	Ti-O equatorial	3.36 (2)	1.968 (2)	0.0003 (1)
	Ti-O axial	1.89(4)	1.976 (2)	0.0003 (1)
	Ti-O_interstitial	1.05(8)	2.620 (7)	0.010 (2)
	Ti-Ti	4.03(3)	3.039 (3)	0.001 (1)
T_800	Ti-O equatorial	3.61(1)	1.961 (2)	0.0002 (1)

	Ti-O axial	2.25 (2)	1.973 (2)	0.0002 (1)
	Ti-O_interstitial	1.28 (9)	2.537 (5)	0.010 (1)
	Ti-Ti	4.41 (2)	3.026 (2)	0.004 (1)
Anatase (Aldrich)	Ti-O equatorial	4.00	1.939 (2)	0.0001 (1)
	Ti-O axial	2.00	1.976 (3)	0.0001 (1)
	Ti-Ti	4.00	3.042 (2)	0.0006 (1)

R – bond distance; σ - XAFS Debye-Waller factor

TOC Graphic